

---

# Image Quality Is Not All You Want: Task-Driven Lens Design for Image Classification

---

Xinge Yang<sup>1</sup> Qiang Fu<sup>1</sup> Yunfeng Nie<sup>2</sup> Wolfgang Heidrich<sup>1</sup>

<sup>1</sup>King Abdullah University of Science and Technology <sup>2</sup>Vrije Universiteit Brussel

## Abstract

In computer vision, it has long been taken for granted that high-quality images obtained through well-designed camera lenses would lead to superior results. However, we find that this common perception is not a "one-size-fits-all" solution for diverse computer vision tasks. We demonstrate that task-driven and deep-learned simple optics can actually deliver better visual task performance. The Task-Driven lens design approach, which relies solely on a well-trained network model for supervision, is proven to be capable of designing lenses from scratch. Experimental results demonstrate the designed image classification lens ("TaskLens") exhibits higher accuracy compared to conventional imaging-driven lenses, even with fewer lens elements. Furthermore, we show that our TaskLens is compatible with various network models while maintaining enhanced classification accuracy. We propose that TaskLens holds significant potential, particularly when physical dimensions and cost are severely constrained.

## 1 Introduction

Modern deep networks have demonstrated exceptional performance across various computer vision tasks, such as image classification [11, 23, 49, 54], object detection [50, 35] and semantic segmentation [24, 53]. To fully exploit their feature extraction capabilities, deep networks typically require sharp, high-quality input images taken by well-designed lenses. However, such lenses can be both costly and structurally complex. For example, modern cellphone lenses usually contain more than five highly aspheric elements [36, 55], and commercial camera lenses [1, 41] usually have more than six precise optical elements.

End-to-End lens design [43, 46] is an emerging technique that optimizes camera lenses and deep networks simultaneously to maximize system performance for specific applications. This approach has demonstrated outstanding results in computational imaging, particularly in extended-depth-of-field [48, 43, 21, 52, 22] and large-field-of-view imaging [33, 48, 21]. More recently, End-to-End designed lenses have been employed in computer vision tasks, such as object detection [7, 46], and have shown superior performance compared to conventional lenses. However, in computer vision tasks, the End-to-End design relies on existing well-corrected lenses as starting points to find a solution. As a result, the End-to-End designed lenses are essentially fine-tuned versions of conventional lenses and improve visual task performance by trading off imaging quality across different fields of view [7, 46]. The well-corrected optical starting points limit the exploration of the design space in optics, preventing the discovery of better lens structures for a given visual task.

To tackle this issue, we propose a novel Task-Driven approach to End-to-End optical design, where we train a network model and fix it to supervise the lens design process. By initializing the lens components of the system from scratch, the Task-Driven approach can simplify the problem and enable the lens to search for a larger solution space. Given that the network has been trained on large datasets, we believe it can extract the most important image features for a visual task. Therefore,

the Task-Driven designed lens only needs to capture these key features from the object space while neglecting the overall imaging quality.

This paper focuses on the image classification task and aims to search for its optimal lens structure. Employing the Task-Driven approach, we design three image classification lenses (“TaskLens”) from scratch without depending on conventional image-quality-based losses, like spot size. Our TaskLens exhibits a novel long-tailed point spread function (PSF) which effectively preserves image features in the presence of optical aberrations for the image classification purpose. For comparison, we design three conventional imaging lenses (“ImagingLens”) for each TaskLens and evaluate their image classification accuracy on ImageNet [8]. The experimental results demonstrate that our TaskLens achieves higher accuracy than ImagingLens with the same number of lens elements. Moreover, our doublet TaskLens outperforms triplet ImagingLens, and our triplet TaskLens outperforms quadruplet ImagingLens. These findings demonstrate that our proposed TaskLens can achieve **better classification accuracy with fewer lens elements**. Additionally, we validate the practical feasibility of our TaskLens through ablation studies.

The contributions of this paper can be summarized as follows:

- We demonstrate that we can design lenses from scratch without relying on or considering any imaging-quality-based losses. Instead, we propose a Task-Driven lens design approach to utilize a well-trained network for supervision.
- Our TaskLens can achieve higher accuracy with even fewer lens elements than conventional ImagingLens. Our TaskLens exhibits a novel long-tail PSF that effectively preserves image features for classification in the presence of optical aberrations.
- We demonstrate that TaskLens is compatible with various network models while maintaining enhanced performance. We also demonstrate that performance improvement can not be achieved through simple image restoration.

## 2 Related Works

**Classical lens design.** Classical lens design methods [17, 18, 40] aim to optimize lenses that fulfill specific imaging quality criteria. The lens optimization process typically involves minimizing image quality-based losses, usually measured by the root-mean-square (RMS) spot size. This refers to the RMS radius of all sampled optical rays within a certain field on the image plane. Smaller RMS spot sizes contribute to enhanced image quality. Ray tracing and optimization algorithms are widely explored in this context and have been extensively applied in optical design software such as Zemax [25] and Code V [44].

**End-to-End lens design.** End-to-End optical design [39, 43, 46, 48] jointly optimizes optical systems (including diffractive, refractive, and reflective components) and downstream image processing networks to enhance the overall capabilities for a target application. It has demonstrated remarkable performance in various applications, including hyperspectral imaging [16, 10, 2, 20], extended-depth-of-field imaging [43, 52, 22, 48], large-field-of-view imaging [33, 48], and seeing through obstructions [38]. End-to-End optical design has also enabled the reduction of optical aberrations in compact structures, such as large field of view [33, 48], and achromatic imaging [39, 10, 34]. Furthermore, it has exhibited improved performance in computer vision tasks over classical lenses, including optical character recognition [5], object detection [46, 7, 5], and depth estimation [3, 15]. However, End-to-End optical design presents challenges for convergence, as both lens design and network optimization are highly non-convex problems. The optical gradients back-propagated from the network are indirect and biased compared to classical lens design objectives (e.g. spot size). To address this challenge, researchers have adopted various strategies, including initiating designs from successful or simple structures [43, 48, 46, 7, 5, 21, 33] or using curriculum learning approaches [52].

**Differentiable image simulation.** In End-to-End optical design, a differentiable optical simulator is necessary to back-propagate the final image loss through the entire pipeline and optimize optical parameters. Existing differentiable optical simulation methods rely on either wave optics or geometric optics. In wave optics, diffractive optical elements (DOEs) [12, 32, 39, 10], metasurfaces [45], and refractive lenses [42, 28, 34, 38, 31] are modeled as phase modulation functions. Refractive lenses are often simplified as thin lenses under the paraxial approximation, which can be inaccurate and fail to represent real lenses. Recent studies in ray tracing-based image simulation [19, 43, 29, 48, 46, 6, 31]

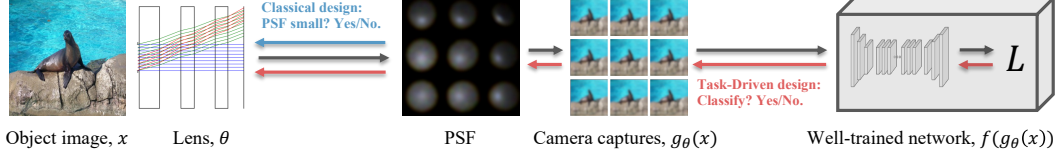


Figure 1: The Task-Driven lens design pipeline involves the computation of PSF through differentiable ray tracing, followed by convolution with input images to simulate camera-captured images at different fields of view. Subsequently, a well-trained network computes the image classification errors and back-propagates the loss function to optimize the lens. Different from classical lens design, Task-Driven lens design focuses on whether the captured images can be successfully classified by the network.

have shown promising accuracy in modeling thick, aspherical lenses and even freeform optics. In this approach, images captured by cameras are simulated using either ray tracing-based rendering or point spread function (PSF) convolution [46, 48, 5, 7]. To make the ray tracing process differentiable, researchers either employ auto-differentiation to compute optical gradients [43, 48, 52, 5, 7] or use a network to represent the optical lens [6, 46, 51].

### 3 Methods

#### 3.1 Task-Driven Lens Design

As shown in Fig. 1, the lens design problem for a visual task can be formulated as follows:

$$\begin{aligned} \theta &= \underset{\theta}{\operatorname{argmin}} \|f(g_\theta(x)) - y\| \\ \text{s.t. } f &= \underset{f}{\operatorname{argmin}} \|f(x) - y\|, \end{aligned} \quad (1)$$

where  $x$  represents the input object image,  $\theta$  represents the lens parameters,  $g$  represents the imaging process,  $f$  represents the target visual task, and  $y$  is the ground truth for the visual task  $f$ . The intuitive solution to Eq. 1 is given by

$$\theta = \underset{\theta}{\operatorname{argmin}} \|g_\theta(x) - x\|, \quad (2)$$

which minimizes the difference between camera-captured image  $g_\theta(x)$  and the object image  $x$ . This imaging-driven classical lens design philosophy guides optical engineers to minimize the PSF of the lens system, corresponding to the blue arrow in Fig. 1.

However, we propose that Eq. 2 represents only a local minimum for the target visual task, as the solution spaces for the visual task and the best imaging quality are different. In particular, we assume that there are key features in the object images for a visual task, and the object image can be decomposed as

$$x = x_f \oplus x_{bg}, \quad (3)$$

where  $x_f$  represents the image features, and  $x_{bg}$  represents the background information. They are combined with the relation  $\oplus$ , but a well-trained network  $f$  can effectively extract  $x_f$  from the input, and only  $x_f$  contributes to the output, formulated as  $f(x) = f(x_f)$ . Based on this assumption, the optical lens only needs to capture/preserve the image features  $x_f$  from the object images:

$$\theta = \underset{\theta}{\operatorname{argmin}} \|g_\theta(x_f) - x_f\|. \quad (4)$$

The philosophy of this Task-Driven design method is to convert the highly non-convex lens optimization problem into a feature encoding problem. As a result, we can neglect the useless background information  $x_{bg}$  and focus on interesting optical features during lens design, rather than minimizing the total aberrations for an intermediate optimal imaging performance as in classical lens design.

Corresponding to the red arrow in Fig. 1,  $x_f$  is determined by a well-trained network  $f$ , which operates as a black box to guide the Task-Driven lens design process. During the optimization, the objective is to generate images that can be successfully classified by the network, without aiming for

perfect imaging quality. It is important to note that Eq. 1–4 are not intended to be strict mathematical proofs; instead, they are used to illustrate our Task-Driven approach.

The Task-Driven lens design pipeline is similar to the End-to-End optical design pipeline, except that we use a well-trained and intact network during the training. Upon the advantages of End-to-End optical methods, we propose this Task-Driven lens design approach mainly based on two observations: (1) the visual capabilities of an End-to-End optical system primarily stem from the optical aspects, and (2) achieving convergence in End-to-End optical design is challenging due to the difficulty of obtaining accurate gradients from an undertrained deep network.

### 3.2 Differentiable Point Spread Function

The PSF characterizes how an optical system blurs a point light source. In image simulation, PSF is convolved with the object image to simulate the camera-captured image. PSF can be computed by ray tracing from a point source to the sensor plane. Subsequently, the optical rays are assigned to their neighboring sensor pixels, as shown in Fig. 2. This process can be formulated as

$$\text{PSF}(\mathbf{o}_p) = \sum_{i=1}^N u_i \cdot \sigma(|(\mathbf{o}_p - \mathbf{o}_i) \cdot \hat{\mathbf{e}}_x|/L) \cdot \sigma(|(\mathbf{o}_p - \mathbf{o}_i) \cdot \hat{\mathbf{e}}_y|/L), \quad (5)$$

where  $\mathbf{o}_p$  denotes the pixel coordinate,  $\mathbf{o}_i$  denotes the intersection position of the  $i$ th ray on the sensor plane,  $N$  represents the numbers of rays from each point source,  $u_i$  denotes the energy, which we assume equals to 1,  $\hat{\mathbf{e}}_x$  and  $\hat{\mathbf{e}}_y$  are unit vector in the sensor plane, and  $L$  denotes the physical width of a sensor pixel. In our experiments, we set  $u_i = 1$ . The  $\sigma$  function is defined as

$$\sigma(x) = \begin{cases} 1 - x & 0 \leq x \leq 1 \\ 0 & \text{otherwise} \end{cases}, \quad (6)$$

which assesses a ray’s impact on its surrounding pixels. As shown in Fig. 2, the total energy of a ray is spread out to its neighboring four pixels. Eq. 5 can be viewed as an inverse bilinear interpolation. By utilizing this sub-pixel information, we can represent the actual light distribution using a limited number of rays. In the backward process, the PSF gradients can guide the rays to move towards the desired pixels as Eq. 5 is differentiable. The gradients can then be back-propagated to adjust the lens surfaces to control the rays.

### 3.3 Implementation Details

In our experiments, we choose 9 distinct fields of view from  $0^\circ$  to full field-of-view (FoV) to represent the comprehensive optical characteristics of the lens. Considering that camera sensors typically have a mega-pixel resolution, while training images have much lower resolutions (e.g.,  $224 \times 224$ ), we treat the training image as patches that appear at different locations in the full-resolution sensor image. We implement the differentiable PSF calculation using a memory-efficient differentiable ray tracer [48, 52]. To accommodate lens dispersion, we use three wavelengths (656.3 nm, 589.3 nm, 486.1 nm) to calculate the PSF of each channel. Furthermore, we utilize a  $51 \times 51$  PSF kernel size to account for significant optical aberrations, also allowing rays to move across a larger region.

The lens surfaces are aspheric, with optimizable parameters of curvature, position, and even polynomial coefficients ranging from  $\alpha_4$  to  $\alpha_{10}$ . Lens materials are chosen from the library of commonly used cellphone lens plastics. The image sensor has a diagonal length of 4 mm and a resolution of  $1080 \times 1920$ , corresponding to a pixel size of  $1.8 \mu\text{m}$ . The AdamW optimizer [27] is employed with a learning rate of  $1e^{-4}$  for curvature, position, and  $\alpha_4$  parameters, while a 0.02 learning rate decay is applied to higher-order polynomial coefficients. In accordance with [52], we

Figure 2: Differentiable PSF computation. Each optical ray is assigned to its neighboring four pixels with a weight term depending on the distance from the ray. The weight term tracks the gradient information and is used to optimize lens parameters during back-propagation.

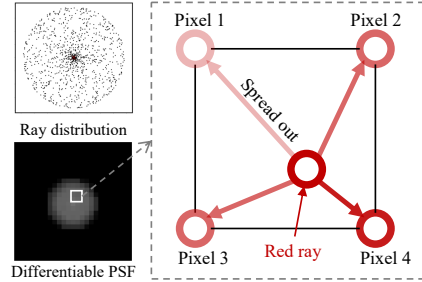


Table 1: Accuracy (top) on the validation set of ImageNet achieved by different lenses. PSNR [dB] (bottom) of simulated camera captures are adopted to represent the imaging quality of the lens. A higher imaging quality does not guarantee a higher classification accuracy.

	TaskLens	ImagingLens #1 / #2 / #3
Doublet	70.08% 19.46	65.63% / 68.54% / 67.01% 22.43 / 23.65 / 22.90
Triplet	73.40% 23.85	70.04% / 69.92% / 68.52% 22.77 / 23.14 / 23.51
Quadruplet	73.61% 23.67	72.27% / 68.88% / 68.56% 25.00 / 23.63 / 23.98

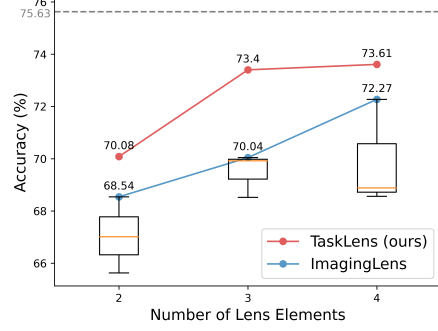


Figure 3: Accuracy comparison between TaskLens and ImagingLens with respect to different numbers of lens elements. Our TaskLens outperforms the ImagingLens even with fewer lens elements.

penalize the incident angles between light rays and lens surfaces to prevent degenerated surface shapes during the initial stages of optimization. Throughout the training process, we sample 256 rays from each field of view to compute the PSF, resulting in a total of approximately  $9$  (fields of view)  $\times$   $256$  (rays)  $\times$   $3$  (channels)  $\approx 7 \times 10^3$  rays.

All images are resized to  $224 \times 224$  and convolved with the PSF to simulate the captured images at that field of view. During training, a batch size of 64 is employed, increasing to 576 after concatenating the image batches for each of the 9 different fields of view. We use TrivialAugment Wide [30] for data augmentation to prevent the learned lens from converging to a perfectly-imaging lens. For the Task-Driven lens design, we utilize a well-trained ResNet50 network [11] for supervision. The lens is optimized from scratch for 1 epoch on the ImageNet training set, typically achieving convergence. Then we conduct End-to-End training to fine-tune the lens. The optimization process consumes approximately 60 GB of GPU memory for a lens and the previous settings, with the bottleneck being the network size and the number of rays.

After designing the lens, we fine-tune the image classification network for each lens using the AdamW optimizer [27] with a learning rate of  $1e^{-5}$  and the CosineAnnealing scheduler [26] with a warm-up scheme. We sample 4096 rays from each field of view during the fine-tuning and testing stages to obtain more accurate PSF. This high sampling rate does not cause memory issues because we do not need to perform differentiable ray tracing at this stage. We fine-tune each network model for an additional 3 epochs, which runs on two 80G A100 GPUs for two days to complete. The classification accuracy is computed on all simulated images at 9 fields of view. Since it would be too expensive if we used the official ImageNet testing set, we split a partition of the training set for validation and use the validation set for testing.

## 4 Task-Driven Image Classification Lens Design

Using our proposed Task-Driven approach, we design three image classification lenses with two, three, and four lens elements from scratch. Each lens has a target FoV of  $68.8^\circ$ , F/2.8, and an image sensor with a 4 mm diagonal length. We control the aperture to F/2.8 by setting the aperture radius to 0.52 mm. Shown in Fig. 4, the Task-Driven approach successfully converges optical rays for valid imaging, although we use a classification network instead of any imaging-based losses.

**Baselines.** For each image classification lens (“TaskLens”), we design three conventional imaging lenses (“ImagingLens”) for comparison. The first ImagingLens (labeled as #1) is optimized under the DeepLens framework [48, 52] by minimizing the spot diagram at different fields of view. The other two ImagingLenses (labeled as #2 and #3) are optimized by experienced (10+ years) optical engineers using ZEMAX [25].

**Classification accuracy comparisons.** Table 1 presents quantitative classification accuracy for all lenses. Our TaskLens demonstrates superior image classification accuracy compared to ImagingLens

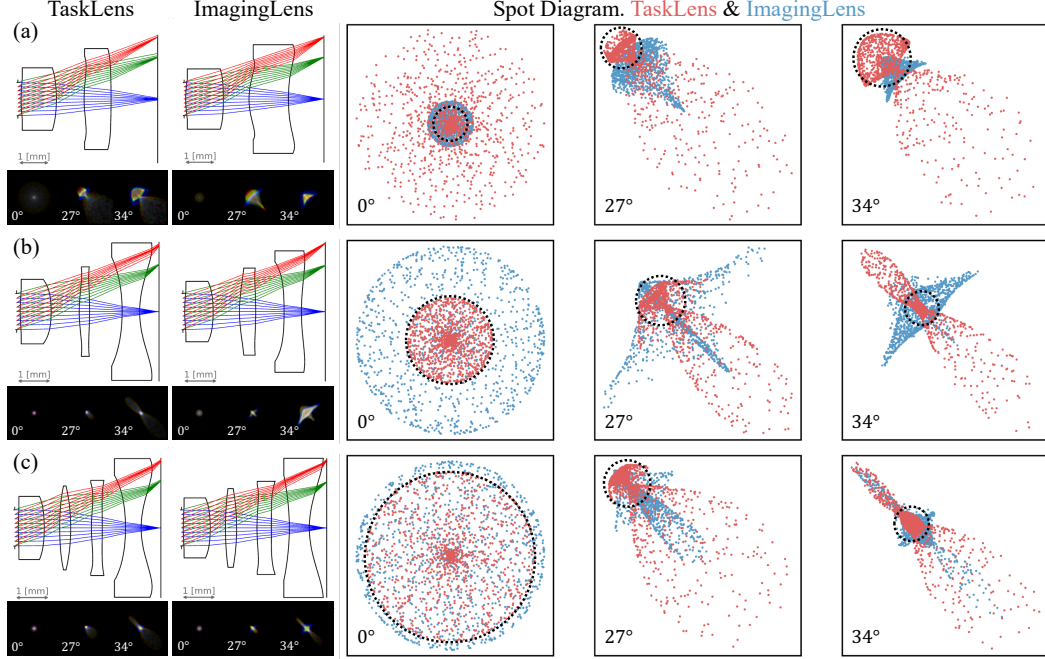


Figure 4: The lens structure, PSF, and spot diagram for doublet (a), triplet (b), and quadruplet (c) lenses. Although the total spot diagram of TaskLens is larger than ImagingLens, the majority of the optical rays converge to a small region, resulting in a smaller effective spot diagram (marked by the black circle). This novel spot diagram leads to a long-tailed PSF, effectively preserving image features from the object images.

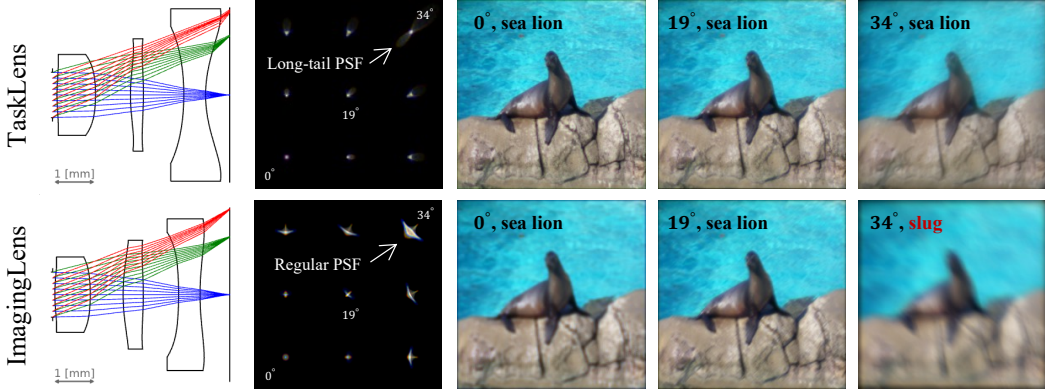


Figure 5: The long-tailed PSF of the TaskLens introduces a haze effect in the captured images while effectively preserving image features. The simulated captures can be successfully classified by the network. In contrast, ImagingLens has a smaller PSF but blends the information, leading to worse classification accuracy.

with the same number of lens elements. The classification accuracy improvement is significant, as shown in Fig. 3. Due to optical aberrations, no lens can reach the upper bound (75.63%) acquired with the original sharp images. Remarkably, our doublet TaskLens outperforms all triplet ImagingLenses, and the triplet TaskLens outperforms all quadruplet ImagingLenses. These results demonstrate that our TaskLens can achieve enhanced image classification accuracy with fewer lens elements compared to conventional lenses.

**Image quality comparisons.** Although image quality is not our design objective and has not been utilized during the Task-Driven design process, we evaluate the image quality for each lens using the PSNR score of simulated camera captures, as presented in Table 1. We find that superior image

quality does not necessarily guarantee enhanced visual task performance, which is in line with our Task-Driven design philosophy.

**Actual optical specifications.** Achieving uniformity in the FoV and effective imaging height across various lens designs can be challenging. To ensure that TaskLens does not exhibit superior visual task performance due to reduced design difficulties, we analyze optical specifications for each lens in Table 2 and compare the design difficulties. The lens design difficulty is correlated with FoV and sensor diagonal distance, and we compute the variations in difficulty relative to the original target parameters (FoV  $68.8^\circ$ , sensor diagonal distance 4 mm) using a linear approximation. Shown in Table 2, our analysis reveals that TaskLens possesses the highest design difficulty, leading us to conclude that the comparison is fair.

#### Explanation for the enhanced visual task performance.

To investigate the reason behind the improvement in classification accuracy, we evaluate the optical characteristics of the TaskLens and the best-performing ImagingLens. We plot the PSF from the optical axis ( $0^\circ$ ) to the full FoV, as well as the corresponding spot diagram at 589.3 nm in Fig. 4. The spot diagram illustrates the intersection points of optical rays and the sensor plane. Due to the insufficient optical elements to correct all optical aberrations, the spot diagram exhibits noticeable optical aberrations. We observe an interesting phenomenon: our TaskLens converges the majority of the optical rays to a small region while neglecting the outlier rays. In contrast, ImagingLens always converges all optical rays towards the center. While the total spot size of the TaskLens is often larger compared to that of the ImagingLens, it is worth noting that when considering the effective spot diagram, the TaskLens demonstrates a smaller spot size compared to the ImagingLens.

This novel spot diagram of TaskLens leads to a distinctive long-tailed PSF at each field of view, particularly for the triplet and quadruplet TaskLenses. As a result, a significant portion of the light energy effectively converges and the valid information in the object images is well preserved. This can be considered as a trade-off between the total spot diagram and the effective spot diagram. The dispersed energy, which creates a haze effect in camera capture (as shown in Fig. 5), can be compensated for by the network. During the training process, the network models can learn to extract valid image features from hazy inputs. Furthermore, it has been demonstrated that network architectures possess an inherent ability to filter out noise and haze[47]. Consequently, the camera captures obtained using TaskLens can still be effectively recognized by the network. In contrast, ImagingLens produces a regular aberrated PSF, which is more uniform compared to the long-tailed PSF. The optical aberrations blend the information present in the object image and result in blurry camera captures (Fig. 5).

## 5 Ablation Study

### 5.1 Can TaskLens Work with Different Classification Models?

In the Task-Driven lens design process, the lens is designed with a specific network model. However, in real-world scenarios, it is common to change downstream network models based on practical constraints. For example, using smaller models to accommodate the limited computational power of end devices or employing larger models to achieve better performance. However, optical lenses cannot be modified after design and manufacturing. Therefore, we aim to investigate whether the visual task performance of TaskLenses is compatible with different network models.

We employ three network models with different model sizes and architectures: MobileNetV3-Large [14] ("MobileNetV3-L") with 5.5M parameters, SwinTransformer-Base [23] ("Swin-B") with 88M parameters, and ViT-Large-patch/16 [9] ("ViT-L/16") with 304M parameters. Additionally, the original ResNet50 network contains 26M parameters. ResNet50 and MobileNetV3-L are convolution

Table 2: Optical configurations for each lens. TaskLens has the highest design difficulty with the same number of lens elements, ensuring a fair comparison.

		FoV	Sensor Diag [mm]	Difficulty
Doublet	TaskLens	$69.5^\circ$ ( $\uparrow 0.7\%$ )	4.0	$\uparrow 1.0\%$
	ImagingLens #1	$69.1^\circ$ ( $\uparrow 0.4\%$ )	4.0	$\uparrow 0.4\%$
	ImagingLens #2	$70.6^\circ$ ( $\uparrow 2.6\%$ )	3.9 ( $\downarrow 2.5\%$ )	$\downarrow 0.1\%$
	ImagingLens #3	$69.5^\circ$ ( $\uparrow 1.0\%$ )	4.0	$\uparrow 1.0\%$
Triplet	TaskLens	$70.7^\circ$ ( $\uparrow 2.8\%$ )	4.0	$\uparrow 2.8\%$
	ImagingLens #1	$69.2^\circ$ ( $\uparrow 0.6\%$ )	4.0	$\uparrow 0.6\%$
	ImagingLens #2	$69.1^\circ$ ( $\uparrow 0.4\%$ )	3.9 ( $\downarrow 2.5\%$ )	$\downarrow 2.1\%$
	ImagingLens #3	$69.1^\circ$ ( $\uparrow 0.4\%$ )	4.0	$\uparrow 0.4\%$
Quadruplet	TaskLens	$70.0^\circ$ ( $\uparrow 1.7\%$ )	4.0	$\uparrow 1.7\%$
	ImagingLens #1	$68.7^\circ$ ( $\downarrow 0.2\%$ )	4.0	$\downarrow 0.2\%$
	ImagingLens #2	$70.6^\circ$ ( $\uparrow 2.6\%$ )	3.8 ( $\downarrow 5.0\%$ )	$\downarrow 2.4\%$
	ImagingLens #3	$69.3^\circ$ ( $\uparrow 0.7\%$ )	4.0	$\uparrow 0.7\%$



Table 3: Classification accuracy with different network models. Our designed TaskLens is compatible with different network models while maintaining enhanced performance. The results for the original ResNet50 are reported in Table 1. Acc Ref: accuracy achieved on original sharp images.

#params / Acc Ref	MobileNetV3-L [13] 5.4M / 73.96%	Swin-B [23] 88M / 85.59%	ViT-L/16 [9] 304M / 86.70%
TaskLens (Doublet)	68.22%	81.19%	81.76%
ImagingLens #1 / #2 / #3	64.60% / 67.73% / 66.05%	79.03% / 80.87% / 80.23%	79.39% / 81.19% / 80.79%
TaskLens (Triplet)	71.82%	82.65%	83.46%
ImagingLens #1 / #2 / #3	68.36% / 67.94% / 68.01%	81.19% / 81.08% / 80.19%	81.62% / 81.46% / 81.61%
TaskLens (Quadruplet)	72.06%	82.82%	83.62%
ImagingLens #1 / #2 / #3	71.00% / 66.78% / 67.19%	82.43% / 80.75% / 80.46%	82.52% / 81.60% / 81.50%

neural networks, while Swin-B and ViT-L/16 are transformer-based architectures. Table 3 presents the image classification accuracy for different models and our TaskLens still holds the highest accuracy at the same number of lens elements. The results demonstrate that our TaskLens is compatible with different network models while maintaining enhanced performance, which also implies that the visual task performance of TaskLens comes from its novel optical characteristics.

Moreover, these results provide inspiration for addressing the memory constraints in Task-Driven lens design by utilizing smaller network models for training. And people can switch to larger models in practice after designing the lens.

## 5.2 Can Image Restoration Bridge the Performance Gap?

Image restoration is commonly employed to mitigate optical aberrations present in camera captures. These algorithms, especially deep learning-based methods, have exhibited remarkable capabilities in recovering fine structures within images, subsequently enhancing the performance of downstream visual tasks. Given the higher level of optical aberrations in our TaskLens compared to conventional ImagingLens, we want to investigate whether the visual task performance gap between TaskLens and ImagingLens can be bridged through image restoration. Consequently, we apply image restoration to all lenses and compare the resulting classification accuracy of the restored images.

Table 4: Classification accuracy after image restoration. The performance gap between TaskLens and ImagingLens can not be bridged by image restoration.

	PSNR [dB]	Classification Acc
TaskLens (Doublet)	27.24	72.03%
ImagingLens	27.54 / 30.30 / 30.87	68.19% / 71.24% / 71.08%
TaskLens (Triplet)	32.31	74.43%
ImagingLens	29.44 / 30.47 / 29.95	72.42% / 73.35% / 70.90%
TaskLens (Quadruplet)	33.58	74.61%
ImagingLens	34.29 / 29.69 / 29.38	73.98% / 72.16% / 71.52%

We employ NAFNet [4] (width = 32, encoding block number = [1, 1, 1, 8], middle block number = 1, and decoding block number = [1, 1, 1, 1]) to recover the camera captures for each lens. We first train the restoration network on camera-captured images to convergence, then fix the restoration network and fine-tune the image classification network using restored images.

Table 4 presents the image restoration and classification results. The image restoration demonstrates an enhancement in classification accuracy for all lenses. However, TaskLens still outperforms ImagingLens with the same number of lens elements. These results suggest that the gap in classification performance cannot be solely bridged by applying image restoration.

## 5.3 Can End-to-End Training Find the Optimal Lens?

In this section, we aim to investigate whether the naive End-to-End optical design approach can identify the optimal lens for image classification. We consider two different starting points: the best-performing ImagingLens and an all-flat lens. The lens, along with a well-trained classification



network (ResNet50), are jointly optimized using the image classification loss. The final classification results are presented in Table 5.

When starting from all-flat optics, the End-to-End training fails to converge. This is primarily due to the inherent difficulty of achieving convergence directly from scratch when utilizing differentiable ray tracing-based imaging models.

On the other hand, when starting with a well-designed imaging lens and network, the system has already reached a local minimum for the visual task. As a result, the gradients back-propagated to the lens parameters are too weak to escape from this local minimum. Consequently, the End-to-End designed lens only fine-tunes the initial starting point (see Supplemental Material), resulting in an inferior classification performance compared to our TaskLens.

Table 5: End-to-End design from scratch fails to converge. While starting with a well-designed ImagingLens, End-to-End design fails to discover the optimal classification lens.

	TaskLens	End2End Training	
		ImagingLens	From scratch
Doublet	70.05%	69.55%	✗
Triplet	73.40%	71.94%	✗
Quadruplet	73.61%	73.44%	✗

## 6 Discussion and Conclusion

**Application scenarios.** In practice, although it is possible to purchase high-quality lenses from the market, there are instances where desired optical specifications such as focal length and FoV are not readily available. Therefore, there is a need to customize lenses but which entails domain-specific expertise, sophisticated manufacturing processes, high costs, and significant leading time. However, with the advance of automatic lens design techniques [52] and 3D printing technology [37], it has become increasingly possible to customize versatile lenses with significantly less effort. By leveraging our proposed Task-Driven lens design approach, we can further simplify the optical structure and reduce the number of lens elements. This reduction in complexity offers the additional benefit of minimizing the effort required in lens customization.

**Limitations.** Our approach also has certain limitations that should be acknowledged. Firstly, the optimization of lens materials is not addressed in our current work, as there are limited options available for cellphone-formed lenses. However, methods proposed in [6, 7] offer potential avenues for material optimization in the future. Secondly, the lens comparison conducted in our study may not be strictly fair in terms of optics. It is important to consider that various factors such as lens manufacturing, manufacturing tolerances, and additional optical properties can impact the overall performance. Unfortunately, at present, we are unable to perform direct manufacturing to evaluate and validate our results.

**Open questions.** The "long-tail" PSF observed in our TaskLens is not exclusive to this paper but has also been observed in End-to-End designed diffractive optics. This "long-tail" PSF has demonstrated effectiveness in various applications, including hyperspectral imaging [2], high-dynamic-range imaging [42], and achromatic imaging [39]. As a result, an open question arises regarding the existence of an optimal PSF for deep-learning-based computational imaging and its efficacy across different applications. This question remains to be explored in the future.

**Conclusion.** In this paper, we introduce a Task-Driven lens design approach that uses a well-trained network to supervise lens design from scratch. We design three lenses for image classification and they outperform the classical imaging-oriented designs with higher classification accuracy. We posit that TaskLens holds considerable potential, particularly in scenarios where physical dimensions and cost are severely constrained.

## References

- [1] Hirofumi Abe. Zoom lens and image pickup apparatus including the same, Apr. 24 2018. US Patent 9,952,446.
- [2] Seung-Hwan Baek, Hayato Ikoma, Daniel S Jeon, Yuqi Li, Wolfgang Heidrich, Gordon Wetzstein, and Min H Kim. Single-shot hyperspectral-depth imaging with learned diffractive optics. In *Proceedings of the IEEE/CVF International Conference on Computer Vision*, pages 2651–2660, 2021.

- [3] Julie Chang and Gordon Wetzstein. Deep optics for monocular depth estimation and 3D object detection. In *Proceedings of the IEEE/CVF International Conference on Computer Vision*, pages 10193–10202, 2019.
- [4] Liangyu Chen, Xiaojie Chu, Xiangyu Zhang, and Jian Sun. Simple baselines for image restoration. *arXiv preprint arXiv:2204.04676*, 2022.
- [5] Shiqi Chen, Ting Lin, Huajun Feng, Zhihai Xu, Qi Li, and Yueting Chen. Computational optics for mobile terminals in mass production. *IEEE Transactions on Pattern Analysis and Machine Intelligence*, 2022.
- [6] Geoffroi Côté, Jean-François Lalonde, and Simon Thibault. Deep learning-enabled framework for automatic lens design starting point generation. *Optics express*, 29(3):3841–3854, 2021.
- [7] Geoffroi Côté, Fahim Mannan, Simon Thibault, Jean-François Lalonde, and Felix Heide. The differentiable lens: Compound lens search over glass surfaces and materials for object detection. *arXiv preprint arXiv:2212.04441*, 2022.
- [8] Jia Deng, Wei Dong, Richard Socher, Li-Jia Li, Kai Li, and Li Fei-Fei. ImageNet: A large-scale hierarchical image database. In *2009 IEEE conference on computer vision and pattern recognition*, pages 248–255. Ieee, 2009.
- [9] Alexey Dosovitskiy, Lucas Beyer, Alexander Kolesnikov, Dirk Weissenborn, Xiaohua Zhai, Thomas Unterthiner, Mostafa Dehghani, Matthias Minderer, Georg Heigold, Sylvain Gelly, et al. An image is worth 16x16 words: Transformers for image recognition at scale. *arXiv preprint arXiv:2010.11929*, 2020.
- [10] Xiong Dun, Hayato Ikoma, Gordon Wetzstein, Zhanshan Wang, Xinbin Cheng, and Yifan Peng. Learned rotationally symmetric diffractive achromat for full-spectrum computational imaging. *Optica*, 7(8):913–922, 2020.
- [11] Kaiming He, Xiangyu Zhang, Shaoqing Ren, and Jian Sun. Deep residual learning for image recognition. In *Proceedings of the IEEE conference on computer vision and pattern recognition*, pages 770–778, 2016.
- [12] Felix Heide, Qiang Fu, Yifan Peng, and Wolfgang Heidrich. Encoded diffractive optics for full-spectrum computational imaging. *Scientific reports*, 6(1):33543, 2016.
- [13] Andrew Howard, Mark Sandler, Grace Chu, Liang-Chieh Chen, Bo Chen, Mingxing Tan, Weijun Wang, Yukun Zhu, Ruoming Pang, Vijay Vasudevan, et al. Searching for MobileNetV3. In *Proceedings of the IEEE/CVF international conference on computer vision*, pages 1314–1324, 2019.
- [14] Andrew G Howard, Menglong Zhu, Bo Chen, Dmitry Kalenichenko, Weijun Wang, Tobias Weyand, Marco Andreetto, and Hartwig Adam. MobileNets: Efficient convolutional neural networks for mobile vision applications. *arXiv preprint arXiv:1704.04861*, 2017.
- [15] Hayato Ikoma, Cindy M Nguyen, Christopher A Metzler, Yifan Peng, and Gordon Wetzstein. Depth from defocus with learned optics for imaging and occlusion-aware depth estimation. In *2021 IEEE International Conference on Computational Photography (ICCP)*, pages 1–12. IEEE, 2021.
- [16] Daniel S Jeon, Seung-Hwan Baek, Shinyoung Yi, Qiang Fu, Xiong Dun, Wolfgang Heidrich, and Min H Kim. Compact snapshot hyperspectral imaging with diffracted rotation. *ACM Transactions on Graphics (TOG)*, 38(4):1–13, 2019.
- [17] Michael J Kidger. Fundamental optical design. In *Fundamental optical design*. SPIE-International Society for Optical Engineering, 2001.
- [18] Rudolf Kingslake and R Barry Johnson. *Lens design fundamentals*. academic press, 2009.
- [19] Craig Kolb, Don Mitchell, and Pat Hanrahan. A realistic camera model for computer graphics. In *Proceedings of the 22nd annual conference on computer graphics and interactive techniques*, pages 317–324, 1995.
- [20] Lingen Li, Lizhi Wang, Weitao Song, Lei Zhang, Zhiwei Xiong, and Hua Huang. Quantization-aware deep optics for diffractive snapshot hyperspectral imaging. In *Proceedings of the IEEE/CVF Conference on Computer Vision and Pattern Recognition*, pages 19780–19789, 2022.
- [21] Zongling Li, Qingyu Hou, Zhipeng Wang, Fanjiao Tan, Jin Liu, and Wei Zhang. End-to-end learned single lens design using fast differentiable ray tracing. *Optics Letters*, 46(21):5453–5456, 2021.
- [22] Yuankun Liu, Chongyang Zhang, Tingdong Kou, Yueyang Li, and Junfei Shen. End-to-end computational optics with a singlet lens for large depth-of-field imaging. *Optics Express*, 29(18):28530–28548, 2021.
- [23] Ze Liu, Han Hu, Yutong Lin, Zhuliang Yao, Zhenda Xie, Yixuan Wei, Jia Ning, Yue Cao, Zheng Zhang, Li Dong, et al. Swin transformer v2: Scaling up capacity and resolution. In *Proceedings of the IEEE/CVF conference on computer vision and pattern recognition*, pages 12009–12019, 2022.
- [24] Ze Liu, Yutong Lin, Yue Cao, Han Hu, Yixuan Wei, Zheng Zhang, Stephen Lin, and Baining Guo. Swin transformer: Hierarchical vision transformer using shifted windows. In *Proceedings of the IEEE/CVF international conference on computer vision*, pages 10012–10022, 2021.
- [25] Zemax LLC. *Zemax User Manual*, 2021.
- [26] Ilya Loshchilov and Frank Hutter. SGDR: Stochastic gradient descent with warm restarts. *arXiv preprint arXiv:1608.03983*, 2016.
- [27] Ilya Loshchilov and Frank Hutter. Decoupled weight decay regularization. *arXiv preprint arXiv:1711.05101*, 2017.
- [28] Christopher A Metzler, Hayato Ikoma, Yifan Peng, and Gordon Wetzstein. Deep optics for single-shot high-dynamic-range imaging. In *Proceedings of the IEEE/CVF Conference on Computer Vision and Pattern Recognition*, pages 1375–1385, 2020.
- [29] Marco Mout, Michael Wick, Florian Bociort, Jörg Petschulat, and Paul Urbach. Simulating multiple diffraction in imaging systems using a path integration method. *Applied optics*, 55(14):3847–3853, 2016.
- [30] Samuel G Müller and Frank Hutter. TrivialAugment: Tuning-free yet state-of-the-art data augmentation. In *Proceedings of the IEEE/CVF international conference on computer vision*, pages 774–782, 2021.

- [31] Yunfeng Nie, Jingang Zhang, Runmu Su, and Heidi Ottevaere. Freeform optical system design with differentiable three-dimensional ray tracing and unsupervised learning. *Optics Express*, 31(5):7450–7465, 2023.
- [32] Yifan Peng, Qiang Fu, Felix Heide, and Wolfgang Heidrich. The diffractive achromat full spectrum computational imaging with diffractive optics. In *SIGGRAPH ASIA 2016 Virtual Reality meets Physical Reality: Modelling and Simulating Virtual Humans and Environments*, pages 1–2. ACM New York, NY, USA, 2016.
- [33] Yifan Peng, Qilin Sun, Xiong Dun, Gordon Wetzstein, Wolfgang Heidrich, and Felix Heide. Learned large field-of-view imaging with thin-plate optics. *ACM Trans. Graph.*, 38(6):219–1, 2019.
- [34] Samuel Pinilla, Seyyed Reza Miri Rostami, Igor Shevkunov, Vladimir Katkovnik, and Karen Egiazarian. Hybrid diffractive optics design via hardware-in-the-loop methodology for achromatic extended-depth-of-field imaging. *Optics Express*, 30(18):32633–32649, 2022.
- [35] Joseph Redmon, Santosh Divvala, Ross Girshick, and Ali Farhadi. You only look once: Unified, real-time object detection. In *Proceedings of the IEEE conference on computer vision and pattern recognition*, pages 779–788, 2016.
- [36] Gal Shabtay, Ephraim Goldenberg, Michael Dror, Itay Yedid, and Gil Bachar. Folded camera lens designs, Feb. 25 2020. US Patent 10,571,644.
- [37] Guangbin Shao, Rihan Hai, and Cheng Sun. 3D printing customized optical lens in minutes. *Adv. Opt. Mater.*, 8(4):1901646, 2020.
- [38] Zheng Shi, Yuval Bahat, Seung-Hwan Baek, Qiang Fu, Hadi Amata, Xiao Li, Praneeth Chakravarthula, Wolfgang Heidrich, and Felix Heide. Seeing through obstructions with diffractive cloaking. *ACM Transactions on Graphics (TOG)*, 41(4):1–15, 2022.
- [39] Vincent Sitzmann, Steven Diamond, Yifan Peng, Xiong Dun, Stephen Boyd, Wolfgang Heidrich, Felix Heide, and Gordon Wetzstein. End-to-end optimization of optics and image processing for achromatic extended depth of field and super-resolution imaging. *ACM Transactions on Graphics (TOG)*, 37(4):1–13, 2018.
- [40] Warren J Smith. *Modern optical engineering: the design of optical systems*. McGraw-Hill Education, 2008.
- [41] Shigenobu Sugita. Zoom lens and image pickup apparatus including same, Aug. 18 2015. US Patent 9,110,278.
- [42] Qilin Sun, Ethan Tseng, Qiang Fu, Wolfgang Heidrich, and Felix Heide. Learning Rank-1 diffractive optics for single-shot high dynamic range imaging. In *Proceedings of the IEEE/CVF conference on computer vision and pattern recognition*, pages 1386–1396, 2020.
- [43] Qilin Sun, Congli Wang, Fu Qiang, Dun Xiong, and Heidrich Wolfgang. End-to-end complex lens design with differentiable ray tracing. *ACM Trans. Graph.*, 40(4):1–13, 2021.
- [44] Inc. Synopsys. Code V, version 13.0. [Software], 2023.
- [45] Ethan Tseng, Shane Colburn, James Whitehead, Luo Cheng Huang, Seung-Hwan Baek, Arka Majumdar, and Felix Heide. Neural nano-optics for high-quality thin lens imaging. *Nature communications*, 12(1):6493, 2021.
- [46] Ethan Tseng, Ali Mosleh, Fahim Mannan, Karl St-Arnaud, Avinash Sharma, Yifan Peng, Alexander Braun, Derek Nowrouzezahrai, Jean-Francois Lalonde, and Felix Heide. Differentiable compound optics and processing pipeline optimization for end-to-end camera design. *ACM Transactions on Graphics (TOG)*, 40(2):1–19, 2021.
- [47] Dmitry Ulyanov, Andrea Vedaldi, and Victor Lempitsky. Deep image prior. In *Proceedings of the IEEE conference on computer vision and pattern recognition*, pages 9446–9454, 2018.
- [48] Congli Wang, Ni Chen, and Wolfgang Heidrich. dO: A differentiable engine for deep lens design of computational imaging systems. *IEEE Transactions on Computational Imaging*, 8:905–916, 2022.
- [49] Wenhai Wang, Jifeng Dai, Zhe Chen, Zhenhang Huang, Zhiqi Li, Xizhou Zhu, Xiaowei Hu, Tong Lu, Lewei Lu, Hongsheng Li, et al. InternImage: Exploring large-scale vision foundation models with deformable convolutions. *arXiv preprint arXiv:2211.05778*, 2022.
- [50] Jianwei Yang, Chunyuan Li, Xiyang Dai, and Jianfeng Gao. Focal modulation networks. *Advances in Neural Information Processing Systems*, 35:4203–4217, 2022.
- [51] Xinge Yang, Qiang Fu, Mohammed Elhoseiny, and Wolfgang Heidrich. Aberration-aware depth-from-focus. *arXiv preprint arXiv:2303.04654*, 2023.
- [52] Xinge Yang, Qiang Fu, and Wolfgang Heidrich. Curriculum learning for ab initio deep learned refractive optics. *arXiv preprint arXiv:2302.01089*, 2023.
- [53] Xiaohua Zhai, Alexander Kolesnikov, Neil Houlsby, and Lucas Beyer. Scaling vision transformers. In *Proceedings of the IEEE/CVF Conference on Computer Vision and Pattern Recognition*, pages 12104–12113, 2022.
- [54] Hao Zhang, Feng Li, Shilong Liu, Lei Zhang, Hang Su, Jun Zhu, Lionel M Ni, and Heung-Yeung Shum. DINO: DETR with improved denoising anchor boxes for end-to-end object detection. *arXiv preprint arXiv:2203.03605*, 2022.
- [55] Xuepeng Zhou. Camera optical lens, Jan. 31 2023. US Patent 11,567,301.